Provided for non-commercial research and education use.
Not for reproduction, distribution or commercial use.

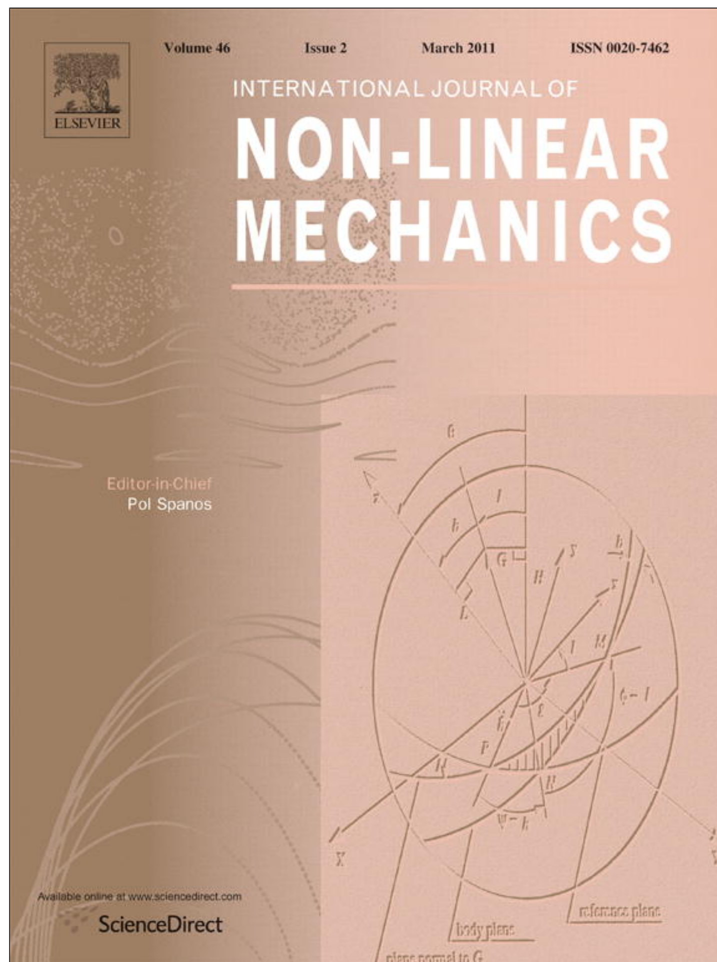

This article appeared in a journal published by Elsevier. The attached copy is furnished to the author for internal non-commercial research and education use, including for instruction at the authors institution and sharing with colleagues.

Other uses, including reproduction and distribution, or selling or licensing copies, or posting to personal, institutional or third party websites are prohibited.

In most cases authors are permitted to post their version of the article (e.g. in Word or Tex form) to their personal website or institutional repository. Authors requiring further information regarding Elsevier's archiving and manuscript policies are encouraged to visit:

http://www.elsevier.com/copyright

Author's personal copy

International Journal of Non-Linear Mechanics 46 (2011) 407–414

Contents lists available at ScienceDirect

International Journal of Non-Linear Mechanics

journal homepage: www.elsevier.com/locate/nlm

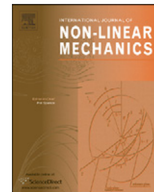

Suppression of pull-in in a microstructure actuated by mechanical shocks and electrostatic forces

Faouzi Lakrad, Mohamed Belhaq *

University Hassan II-Casablanca, Laboratory of Mechanics, Casablanca, Morocco

ARTICLE INFO

Article history:
Received 2 September 2009
Received in revised form
28 October 2010
Accepted 29 October 2010

Keywords:
Pull-in
Capacitive MEMS
High-frequency voltage
Shock
Control

ABSTRACT

This work investigates the effect of a high-frequency voltage (HFV) on the pull-in instability in a microstructure actuated by mechanical shocks and electrostatic forces. The microstructure is modelled as a single-degree-of-freedom mass-spring-damper system. The method of direct partition of motion is used to split the fast and slow dynamics. Analysis of steady-state solutions of the slow dynamic allows the investigation of the influence of the HFV on the pull-in. The results show that adding HFV rigidifies the system, creates new stable equilibria and suppresses the pull-in instability for adequate high-frequency voltages. To illustrate the applicability of the result, a specific capacitive microelectromechanical system consisting of a clamped–clamped microbeam is considered.

© 2010 Elsevier Ltd. All rights reserved.

1. Introduction

Analysis of vibrational behavior of Microelectromechanical systems (MEMS) is an active topic of research with applications in many engineering fields such as communications, automotive, robotics and others. One of the most critical issues in the design of MEMS is their reliability and survivability under mechanical shocks and electrical loads. In the case of capacitive MEMS devices the pull-in [1–3] constitutes one of the main roots to the device failure. Pull-in is a structural instability phenomenon resulting from the interaction between elastic and electrostatic forces in MEMS devices. This instability results from the unbalance between the electric actuation and the mechanical restoring force leading a movable electrode to hit a stationary electrode causing stiction and short circuit problems and hence the failure in the device's function [4]. Several works [5,6] investigated the static pull-in phenomenon and performed techniques to predict its occurrence by determining the largest DC voltage for which the system operates in a stable behavior. The dynamic pull-in was studied under various loads, such that step voltage [7], AC harmonic voltage [8,9] and mechanical shock load [10,11]. It was shown that the dynamic actuation reduces drastically the static pull-in threshold. Nayfeh and co-workers [8,9] studied the dynamic pull-in of MEMS resonators actuated by a resonant AC voltage. They found three distinct mechanisms leading to the dynamic pull-in instability. The first mechanism is the cyclic-fold or symmetry instabilities, the second mechanism depends on the system transient dynamics and the number of coexisting attractors and the third one is characterized by the sensibility to initial conditions due to the existence of homoclinic tangles. Moreover, Younis and co-workers [10,11] showed that the combination of a shock load and an electrostatic actuation makes the instability threshold much lower than the threshold predicted considering the effect of the shock alone or the electrostatic actuation alone. They also studied the effects of the shape of the shock pulse and its duration on the pull-in threshold. Recently, Ibrahim and Younis [12] presented a theoretical and experimental investigation of the response of electrostatically actuated parallel-plate resonators subjected to mechanical shocks. They concluded that a resonator may experience early dynamic pull-in instability depending on the shock duration.

Keeping a MEMS device operating in a stable attracting regime away from the pull-in instability limit presents a major interest from design, fabrication process and commercialization point of view. This challenge has motivated researchers developing strategies to avoid the pull-in, and hence, increase the range of movable electrode. For example, Castañer et al. [13] used an interesting technique based on charge control, instead of voltage control. This method allows extending the travel range, but it is limited by the charge pull-in [14]. Lenci and Rega [15] used a control method based on adding superharmonics to a reference harmonic excitation and showed the possibility of shifting the dynamic pull-in towards high excitation amplitudes. Lakrad and Belhaq [16] showed that applying an appropriate high-frequency harmonic voltage can delay the static pull-in.

In the present paper, a HFV is used to suppress the pull-in instability induced by the combined effect of electrostatic and shock forces. The proposed method is applied to a simplified mass-spring-damper

* Corresponding author.
E-mail address: mbelhaq@yahoo.fr (M. Belhaq).

0020-7462/$ - see front matter © 2010 Elsevier Ltd. All rights reserved.
doi:10.1016/j.ijnonlinmec.2010.10.006

Author's personal copy

system modelling the dynamic of a capacitive MEMS. It is worth noting that the problem of studying the effects of high-frequency excitations on the dynamic of mechanical systems has been examined during the last decade by a number of authors; see for instance [17] and references therein. Attention was focused on the effect of high-frequency excitations on the natural frequencies [18,19], symmetry breaking [20], limit cycles [21], hysteresis [22,23] and pull-in instability [16].

The rest of the paper is organized as follows. The equation of motion modelling the dynamic of the MEMS device is presented as a mass-spring-damping oscillator in Section 2. Then, the method of direct partition of motion is performed on the oscillator over the fast dynamic and the main equation governing the slow dynamic of the MEMS device is derived. In Section 3, we expose the main analytical and numerical results of our study, while in Section 4 an application to a real capacitive MEMS is considered. Section 5 concludes the work.

2. Formulation of the problem and slow dynamic

Consider the following non-dimensional equation

$$X''+2\xi X'+X=\frac{\alpha}{(1-X)^2}+\frac{\beta\cos(\Omega\tau)}{(1-X)^2}+f_0 g(\tau) \tag{1}$$

representing a single-degree-of-freedom model of a capacitive MEMS device employing a DC and AC voltages as actuator and subjected to a mechanical shock. The primes denote the derivatives with respect to the non-dimensional time τ, X is the normalized displacement with respect to the initial gap of the movable mass and ξ is the damping coefficient. The amplitude and the pulse shape of the shock are denoted by f_0 and $g(\tau)$, respectively. Note that $X=1$ corresponds to the pull-in and the left hand side of Eq. (1) is considered as a linear mechanical oscillator. However, non-linearities can arise in the mechanical subsystem through non-linear mechanical stiffness. The choice of considering a linear mechanical model can be justified by the fact that the thickness of the movable electrode is greater than the initial gap. The first term in the right hand side of Eq. (1) represents the effect of the DC voltage, the second term is related to the AC actuation and the last one describes the effect of the shock load. The parameters α and β are first treated as independent entities in the analysis, even though they are related in real capacitive MEMS. This does not impact our results as shown in Section 4. Note that in [16] the authors shown that it is possible, in this case, to prevent the electrostatically induced pull-in instability for a range of values of the amplitude and the frequency of the high-frequency AC. The high-frequency Ω is normalized with respect to the natural frequency and is taken very large with respect to unity. In this paper, we consider that the natural period T_p of the microstructure is very small compared to the duration T of the shock. Consequently, the shock force is experienced as a quasi-static force that stays for some time and is then removed [10].

Eq. (1) contains a slow dynamic which describes the main motion at time-scale of the microstructure natural vibration and a fast dynamic at time-scale of the high-frequency voltage. To obtain the main equation governing the slow dynamic of the device, we implement the method of direct partition of motion [17]. Two different time-scales are introduced: a fast time $T_0=\eta^{-1}\tau$ and a slow time $T_1=\tau$ and the displacement of the mass $X(\tau)$ is split up into a slow part $Z(T_1)$ and a fast part $\phi(T_0,T_1)$ as follows:

$$X(\tau)=Z(T_1)+\phi(T_0,T_1)=Z(T_1)+\eta^2\tilde{\phi}(T_0,T_1) \tag{2}$$

Here the positive parameter η is introduced to measure the smallness of other parameters ($0<\eta\ll 1$). The slow part $Z(T_1)$ takes into account the transient motion composed of the natural damped motion of the microstructure and the response to the shock force. The high-frequency is taken as $\Omega=\eta^{-1}$. The fast motion and its derivatives are assumed to be $2\pi-$periodic functions of the fast time T_0 with zero mean value with respect to it. Thus, $\langle X(\tau)\rangle=Z(T_1)$ where $\langle . \rangle=(1/2\pi)\int_0^{2\pi}(.)dT_0$ defines the fast time-averaging operator. Introducing $D_m^n=\partial^n/\partial T_m^n$ yields

$$\frac{d}{d\tau}=\eta^{-1}D_0+D_1+O(\eta) \tag{3}$$

$$\frac{d^2}{d\tau^2}=\eta^{-2}D_0^2+\eta^{-1}2D_0D_1+D_1^2+O(\eta) \tag{4}$$

Substituting (3) and (4) into (1) leads to the following equation

$$\begin{aligned}&(D_0^2\tilde{\phi})+2\eta(D_0D_1\tilde{\phi})+\eta^2(D_1^2\tilde{\phi})+(D_1^2 Z)\\&\quad+2\xi[(D_0\tilde{\phi})+\eta(D_1\tilde{\phi})+(D_1Z)]+Z+\eta^2\tilde{\phi}\\&=\frac{\alpha}{(1-Z-\eta^2\tilde{\phi})^2}+\frac{\beta\cos(T_0)}{(1-Z-\eta^2\tilde{\phi})^2}+f_0g(T_1)\end{aligned} \tag{5}$$

In what follows we set $\beta=O(1)$ and $\xi=\eta\tilde{\xi}$. All the parameters with tildes are of order $O(1)$.

The dominant terms depending on T_0 up to the order $O(1)$ in (5) are

$$(D_0^2\tilde{\phi})=\frac{\beta}{(1-Z-\eta^2\tilde{\phi})^2}\cos(T_0) \tag{6}$$

Thus, up to this leading order, the fast motion is given by

$$\tilde{\phi}(T_0,T_1)=-\frac{\beta}{(1-Z)^2}\cos(T_0)+O(\eta) \tag{7}$$

Now averaging Eq. (5) over a period of the fast time scale T_0 leads to the following equation

$$\begin{aligned}&(D_1^2Z)+2\xi(D_1Z)+Z\\&=\left\langle\frac{\alpha}{(1-Z-\eta^2\tilde{\phi})^2}+\frac{\beta\cos(T_0)}{(1-Z-\eta^2\tilde{\phi})^2}\right\rangle+f_0g(T_1)\end{aligned} \tag{8}$$

where

$$\left\langle\frac{\alpha}{(1-Z-\eta^2\tilde{\phi})^2}\right\rangle=\frac{\alpha}{(1-Z)^2}+O(\eta^3) \tag{9}$$

$$\left\langle\frac{\beta}{(1-Z-\eta^2\tilde{\phi})^2}\cos(T_0)\right\rangle=-\frac{\beta^2}{\Omega^2(1-Z)^5}+O(\eta^3) \tag{10}$$

The equation of the slow dynamics up to the order $O(\eta^3)$ can be written as

$$(D_1^2Z)+2\xi(D_1Z)+Z=\frac{\alpha}{(1-Z)^2}-\frac{\beta^2}{\Omega^2(1-Z)^5}+f_0g(T_1) \tag{11}$$

Eq. (11) governs the transient slow dynamics of the movable electrode and can be used to study the pull-in instability in the presence of a high-frequency harmonic actuation. The present work focuses attention only on steady-state equilibria. Through Eq. (11) one can conclude that the DC voltage is softening the structure while the HFV is hardening it. As a consequence, increasing β will increase the natural frequency of the structure and will damp quickly its free vibrations. It is worth noting that the zeros of the slow dynamic, Eq. (11), in the absence of the shock or after the end of its effect, are the periodic solutions of Eq. (1). These zeros are obtained by solving the following sixth order algebraic equation

$$Z(1-Z)^5=\alpha(1-Z)^3-\frac{\beta^2}{\Omega^2} \tag{12}$$

It is clear that in the absence of the HFV i.e., for $\beta=0$, the steady-state equilibria are obtained by solving $Z(1-Z)^2=\alpha$. The static pull-in in this case is obtained for the static tension $\alpha_p=\frac{4}{27}=0.148$ which corresponds to the steady state displacement $Z_p=\frac{1}{3}$.

Author's personal copy

3. Pull-in analysis

In this section, we analyze the effect of different actuations on the pull-in instability using the slow dynamic, Eq. (11), and numerical simulations of Eq. (1).

3.1. Effect of the electrostatic force alone

In this subsection, we begin by analyzing the response of the system to a DC voltage alone. The DC polarization is used to achieve permanent displacements of the mass. The damping coefficient is taken $\xi=0.1$ in all computations. In Fig. 1, the normalized displacement to the gap $X(\tau)$ is shown for $\alpha=0.1$. Note that the steady-state amplitude is near $X=0.133$. We recall that the instability limit according to the static analysis is $X=1/3$. In Fig. 2, the time history of (1) is shown for $\alpha=0.15$ which corresponds to a post pull-in threshold value. This instability is characterized by the slope of the displacement approaching infinity.

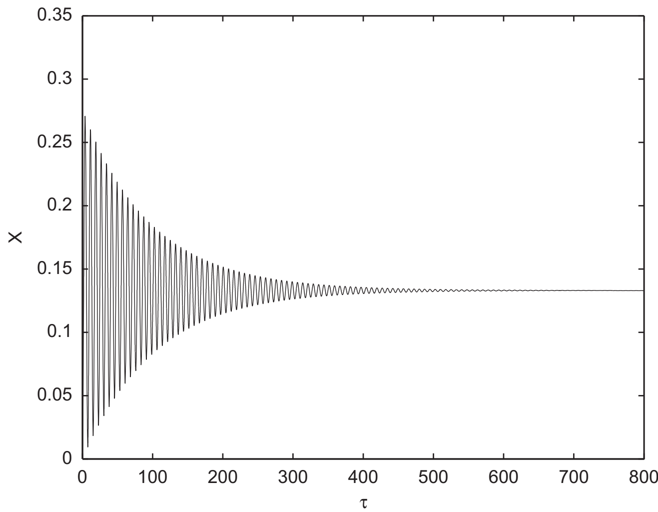

Fig. 1. Time history of Eq. (1) for $\xi=0.1$, $\alpha=0.1$, $\beta=0$ and $f_0=0$.

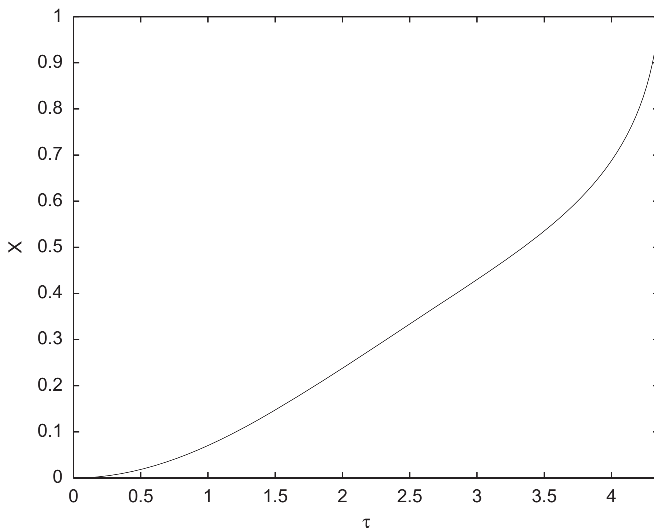

Fig. 2. Time history of Eq. (1) for $\xi=0.1$, $\alpha=0.15$, $\beta=0$ and $f_0=0$.

3.2. Effect of the shock combined to the electrostatic force

The shock force is characterized by its shape, amplitude and the duration. In what follows the shock force is assumed to be a half-sine shock pulse (see Fig. 3) which is expressed as

$$g(t)=\sin\left(\frac{\pi}{T}t\right)[u(t)-u(t-T)] \tag{13}$$

In terms of the non-dimensional time τ, the shock shape is written as

$$g(\tau)=\sin(r\tau)\left[u\left(\frac{rT}{\pi}\tau\right)-u\left(\frac{rT}{\pi}\tau-T\right)\right] \tag{14}$$

Here $r=T_p/(2T)$, $T_p=2\pi/\omega$ is the natural period of the microsystem, T is the shock duration and $u(t)$ is the unit step function. As stated in the previous section, we consider that the natural period T_p of the microstructure is very small compared to the duration of the shock T. Consequently, for numerical applications, $r=0.01$ and the duration of the shock is taken $T=1.0$ ms. In Fig. 4, the normalized displacement $X(\tau)$ is computed, when the microstructure is actuated by the shock alone, for various values of the shock amplitude f_0. It is worth noting that the response of the microstructure takes a similar shape to the shock pulse profile. The increase of the shock amplitude causes the increase of the maximum displacement of the microstructure

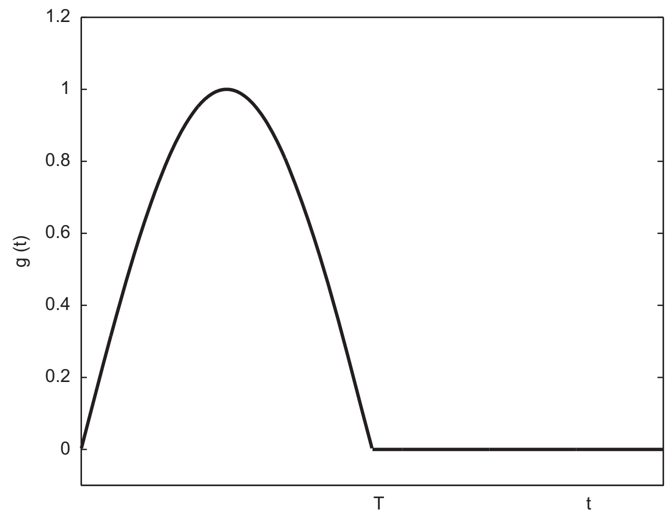

Fig. 3. Half-sine shock pulse.

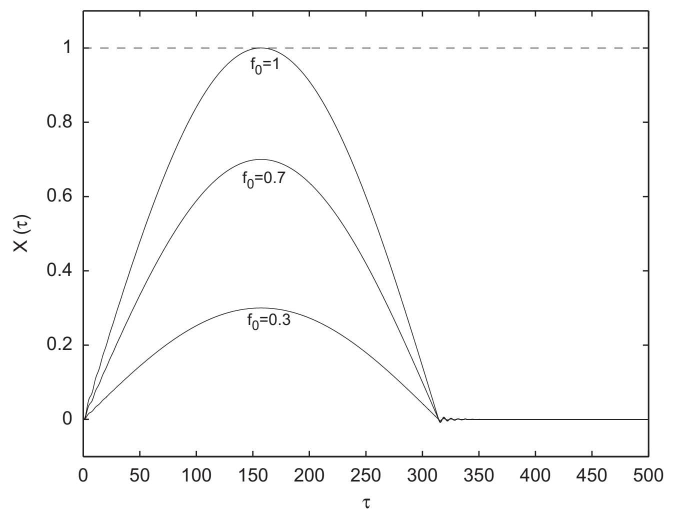

Fig. 4. Response of the mass actuated by a shock alone for various values of f_0.

Author's personal copy

linearly till touching the stationary electrode. The shock amplification factor causing the pull-in is $f_{0p}=1$.

In the presence of electrostatic forces, a stable system which operates far from the instability threshold, can go unstable under the effect of a shock load that is moderate in magnitude i.e., for $f_0 \ll 1$; see [10] for more discussions. As a consequence, the microstructure is vulnerable under the combination of a shock force and a DC voltage. This fact is illustrated in Fig. 5 where the pull-in instability threshold is shown in the plane (α, f_0) for $\beta=0$ and $\xi=0.1$. This figure is obtained by numerical integration of Eq. (1) with the movable mass initially in rest.

3.3. *Effects of the HFV and the electrostatic force*

First, we consider the effect of the HFV in the absence of the static tension i.e., for $\alpha=0$. In Fig. 6, the time response of Eq. (1), including the transient behavior, is plotted for various values of the amplitude β of the HFV and for $\Omega=10$. As expected, the time history of the stationary response is periodic with the same period as the HFV. It is also noted from this figure that the vibration of the mass occurs around a reference position which corresponds to the steady-state position of the slow dynamic. Thus, it is obtained by solving Eq. (12) for $\alpha=0$ i.e., by solving the following algebraic equation

$$Z(1-Z)^5 = -\frac{\beta^2}{\Omega^2} \tag{15}$$

Furthermore, the reference position shifts in the opposite direction to the stationary electrode when β is increased. This result is illustrated in Fig. 7 for $\Omega=10$. The stars denote the averaged positions of the mass displacement computed through the numerical integration of Eq. (1) and using $(\max(X(\tau))+\min(X(\tau)))/2$. The continuous line is obtained by solving the algebraic Eq. (15) giving the steady-state positions of the slow dynamic. The reported steady-state oscillations evolving towards negative-valued equilibria are due to the high-frequency actuation that produces a hardening effect on the electrode. This fact was largely discussed in [17].

In Fig. 8, the shift of the steady-state position, with respect to the non-deformed position $X=0$, is computed versus the frequency Ω for $\beta=10$. It can be seen from this figure that increasing the frequency Ω causes the shift to decrease. Note that the trend shown in Fig. 8 for $\beta=10$ is preserved for small values of β.

This preliminary analysis indicates that the HFV rigidifies the microstructure and shifts its reference position to the opposite

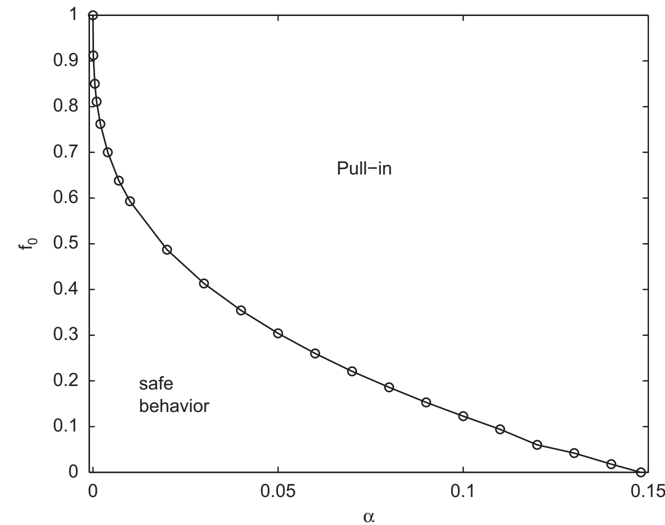

Fig. 5. Pull-in threshold in the plane (α, f_0) for $\beta=0$ and $\xi=0.1$.

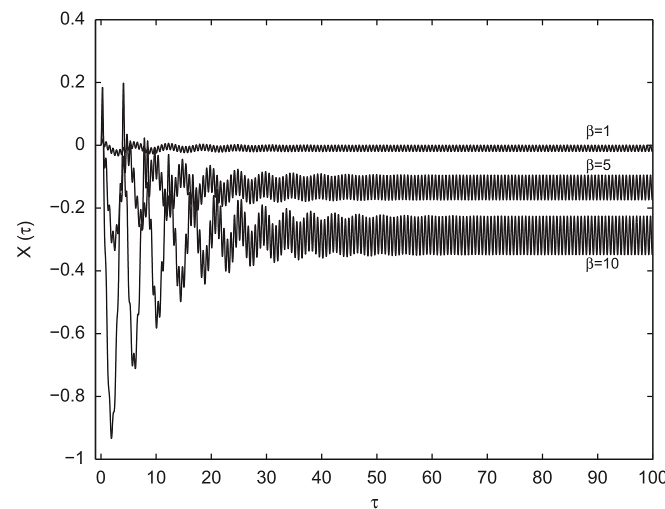

Fig. 6. Time history of (1) for $\alpha=0, f_0=0, \Omega=10$ and for increasing values of β.

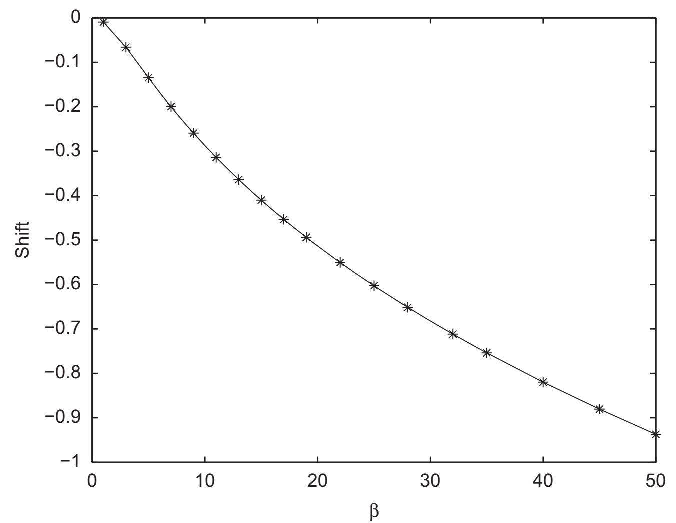

Fig. 7. Shift of the averaged position versus β for $\Omega=10$, $\xi=0.1$ and $\alpha=0$.

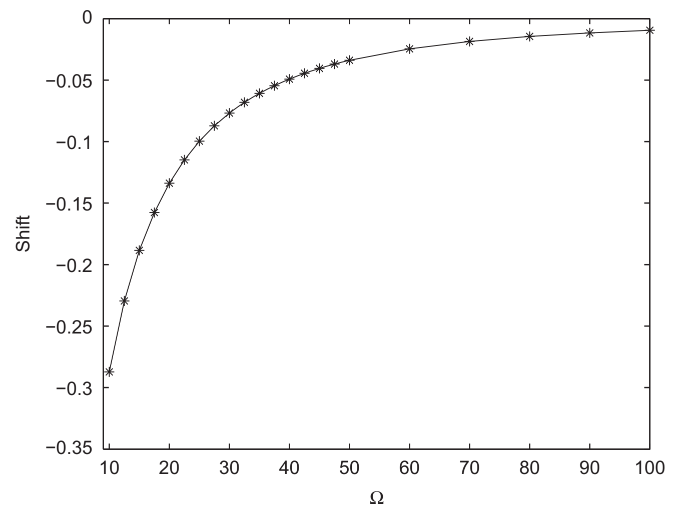

Fig. 8. Shift of the averaged position versus Ω for $\beta=10$, $\xi=0.1$ and $\alpha=0$.

Author's personal copy

direction of the substrate, namely in the opposite direction of the pull-in instability. Thus, it is convenient to take advantage of this non-trivial effect to enable the microstructure vibrating in a stable solution for parameters values greater than the static pull-in voltage. To this end, we consider the case where the mass is in the post pull-in state caused by a DC tension $\alpha = 0.15$. Fig. 9 depicts for $\Omega = 10$ the stationary solutions of the slow dynamics, Eq. (12), (in continuous line) and the numerically computed reference positions (in circles) of the periodic solutions of Eq. (1) versus β. It can be seen from this figure that for increasing values of β, there is a periodic stable response of the microstructure in the safe range i.e., $X(\tau) < 1$.

In Fig. 10 the quasi-static solution given by Eq. (12) (lines) and the averaged position of Eq. (1) (circles) are shown versus Ω. For $\Omega < 168$, there is one stable solution in the range $Z < 1/3$. For $\Omega = 168$, a saddle-node bifurcation gives birth to two other solutions, one is stable and the other one is unstable (dashed line). The new stable solution stands in the range $Z > 0.5$. Thus, in the range $169 < \Omega < 428$, there is coexistence of two stable solutions. For $\Omega > 428$, the lower stable solution disappears by a saddle-node bifurcation leaving only one solution which approaches asymptotically the pull-in position $Z=1$ as Ω increases. These results are confirmed by computing numerically the averaged position of Eq. (1). In Fig. 11 are shown the coexisting stable solutions of Eq. (1) for $\Omega = 250$ picked from Fig. 10. The upper solution corresponds to the initial condition (0,0) and the lower one corresponds to (0.25,0).

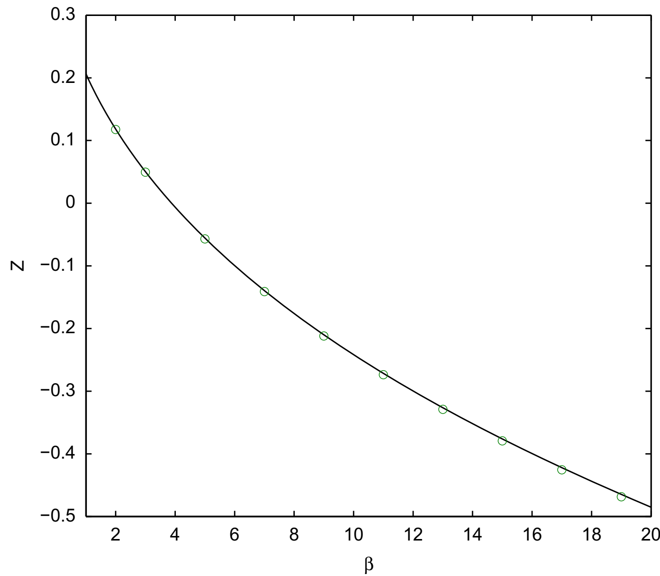

Fig. 9. Stationary solutions of the slow dynamic versus β for $\Omega = 10$, $\xi = 0.1$ and $\alpha = 0.15$. Continuous lines correspond to steady-state solutions of (12) and circles correspond to averaged positions of (1).

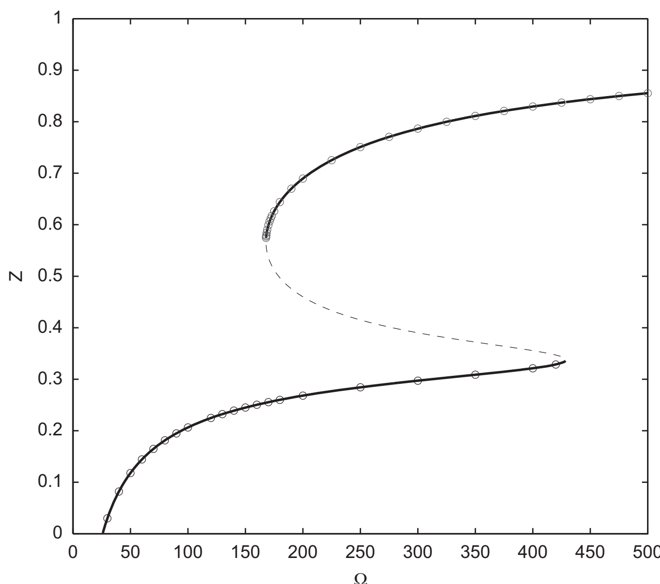

Fig. 10. Stationary solutions of the slow dynamic versus Ω for $\beta = 10$ and $\alpha = 0.15$. Continuous and dashed lines correspond to stable and unstable solutions, respectively. Circles correspond to averaged positions of (1).

3.4. *Effect of the HFV on the pull-in caused by a shock and a DC voltage*

In what follows we investigate the effect of the HFV on a post pull-in state. For the next numerical simulations, the amplitude of the shock and the DC voltage are taken $f_0=2$ and $\alpha = 0.2$, respectively. These values represent a harsh environment which corresponds to a shock having an amplitude two times the shock amplitude causing the pull-in i.e., $f_{0p}=1$ and a DC voltage higher than the pull-in voltage $\alpha_p = 0.148$.

Figs. 12 and 13 show time histories of the slow dynamic given by Eq. (11) (in grey) and time histories of Eq. (1) (in black) for $\Omega = 60$ and for different values of β. It can be seen from these figures that the response tends to stationary solutions after the end of the shock effect. These stationary solutions are, respectively, $Z=0.236$ and 0.745 and are obtained by solving the algebraic Eq. (12). As expected, the solution of the microstructure is composed of a high-frequency response oscillating around the slow dynamic solution. These figures illustrate suppression of the pull-in by the HFV. Moreover, it is shown through these time histories that increasing β leads to damping faster the transient vibrations.

In Fig. 14 is shown the zones of pull-in suppression (grey zone) in the plane (β,Ω). In this figure, the DC voltage and the shock force have values far beyond the pull-in threshold i.e., $\alpha = 0.2$ and $f_0=2$. The threshold values of this zone are computed by integrating Eq. (1) taking as initial conditions the zeros of Eq. (12) in the absence of shocks. Fig. 14 indicates that the amplitude β corresponding to the pull-in suppression threshold increases when Ω decreases.

4. Application to a real capacitive MEMS

In a real MEMS the AC tension amplitude cannot exceed the DC voltage, i.e., $\beta \le \alpha$. In what follows this condition will be taken into

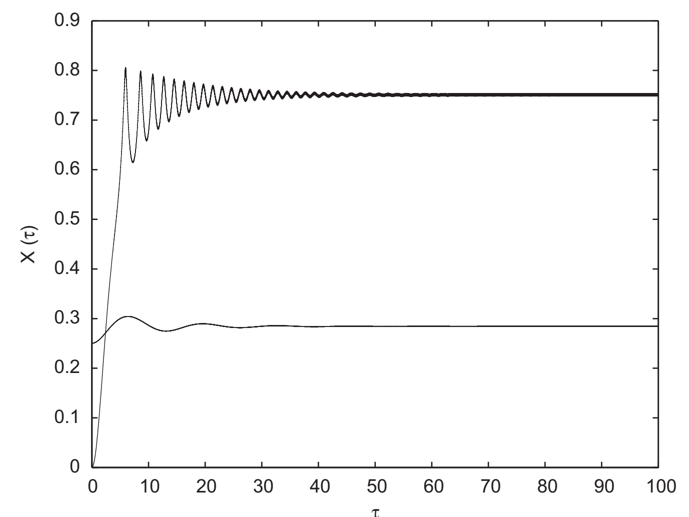

Fig. 11. Time history of coexisting stable solutions of (1) for $\Omega = 250$, $\beta = 10$, $\xi = 0.1$ and $\alpha = 0.15$.

Author's personal copy

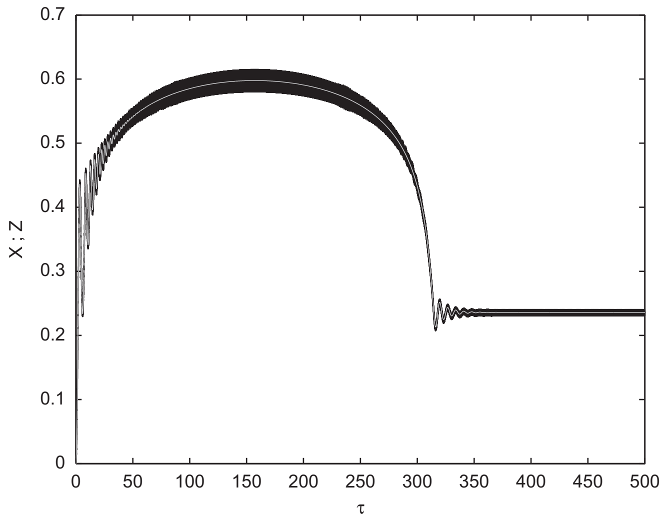

Fig. 12. Time histories for $\alpha=0.2$, $f_0=2$, $\beta=10$, $\xi=0.1$ and $\Omega=60$: in grey solution of Eq. (11) and in black solution of Eq. (1).

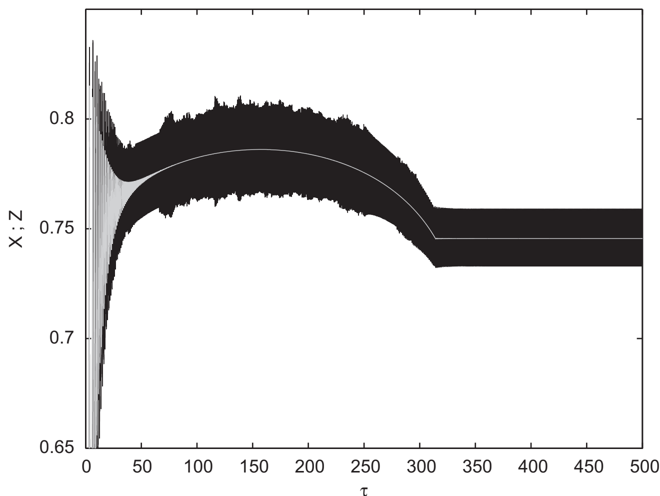

Fig. 13. Time histories for $\alpha=0.2$, $f_0=2$, $\beta=3$, $\xi=0.1$ and $\Omega=60$: in grey solution of Eq. (11) and in black solution of Eq. (1).

consideration and consequently, the effect of the HFV will not be as strong as in the mathematical model studied in the previous sections. In Fig. 15 is shown the natural frequency of the oscillator under the electrostatic force versus α. This figure is obtained by numerically integrating Eq. (1) for $\beta=0$ and $f_0=0$ and then an FFT program is used to determine the natural frequencies. This figure indicates that increasing α softens the oscillator leading the natural frequency of the system to decrease.

In Fig. 16 are shown the time histories of Eq. (1) for $\beta=0.109$ and for various values of Ω. It is shown that the introduction of a HFV of amplitude $\beta=\alpha$ delays the time of the pull-in for $\Omega=10$ and suppresses it for $\Omega=5$.

In Fig. 17 are plotted the thresholds of the pull-in in the plane (α,f_0) in the absence of the HFV (the lower continuous line) and in the presence of the HFV for $\beta=\alpha$ and $\Omega=5$ (the higher continuous line). The grey zone corresponds precisely to the zone where the HFV suppresses the pull-in. Fig. 17 is obtained through numerical integration of Eq. (1) for trivial initial conditions.

Based on the previous results, we claim that the pull-in of a clamped–clamped microbeam made of Silicon [10], caused by the combination of an electrostatic force and a mechanical shock, can be

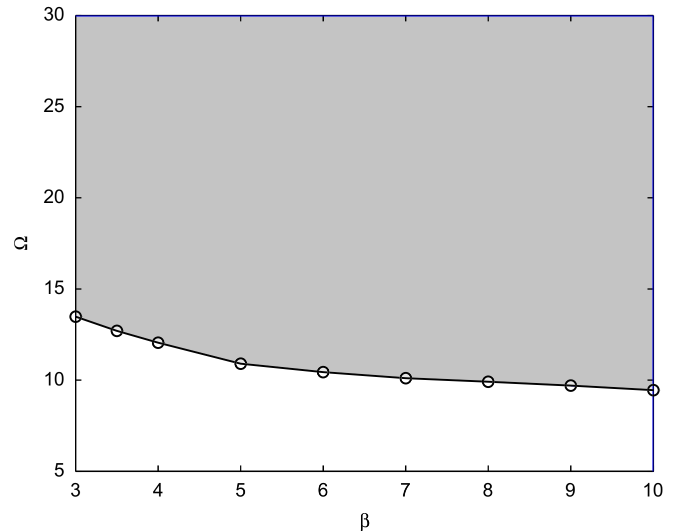

Fig. 14. Zone of suppression (grey zone) of the pull-in in the plane (β,Ω) for $\alpha=0.2$, $\xi=0.1$ and $f_0=2$. Slow dynamic, Eq. (11), (line) and original Eq. (1) (circles).

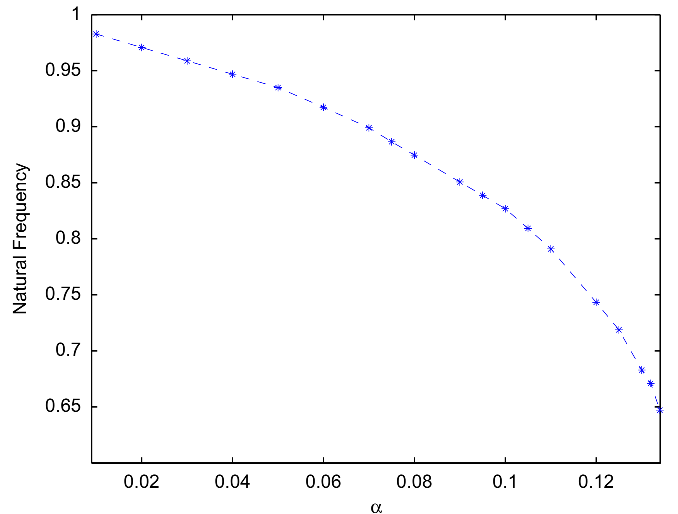

Fig. 15. Natural frequency of the oscillator versus α in the absence of HFV.

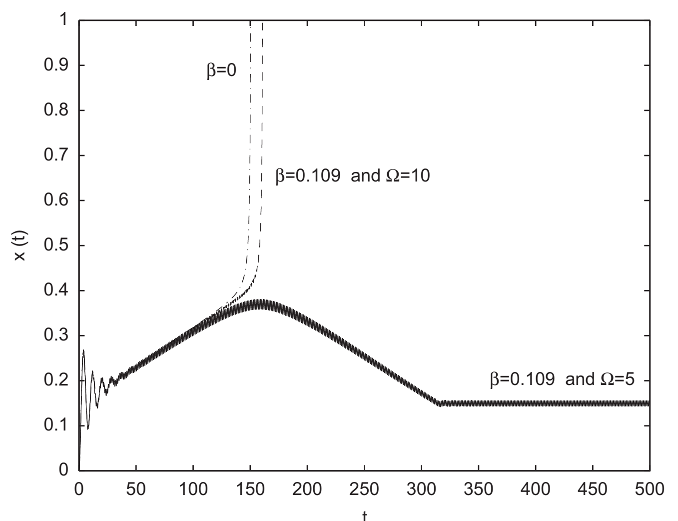

Fig. 16. Time histories of Eq. (1) for various values of β and Ω.

Author's personal copy

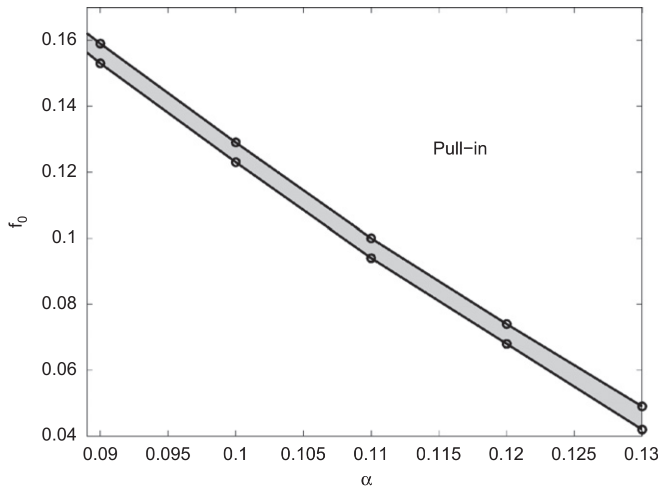

Fig. 17. Threshold of pull-in in the plane (α,f_0) for $\xi=0.1$, in the absence of HFV (lower curve) and in the presence of HFV (higher curve) for $\beta=\alpha$ and $\Omega=5$. The grey zone is the zone where the pull-in is suppressed.

suppressed using an adequate HFV. This can be shown considering the following real capacitive MEMS consisting in the microbeam having the geometrical properties as in [10]: the length $L=510$ μm, the thickness $h=1.5$ μm, the width $b=100$ μm and the gap width $d=1.18$ μm. In this case the fundamental natural frequency of the microstructure is 50.464 kHz. Furthermore, following [24] an input voltage in the form $V(t)=V_{dc}\sqrt{1+\cos(\Omega t)}$ is considered. In this case the DC voltage and the AC voltage are taken equal. Thus, the non-dimensional parameters are given by

$$\alpha=\frac{\varepsilon A}{2m\omega^2 d^3}V_{dc}^2 \tag{16}$$

$$\beta=\frac{\varepsilon A}{2m\omega^2 d^3}V_{dc}^2 \tag{17}$$

$$f_0=\frac{F_0 g}{\omega^2 d} \tag{18}$$

where m is the mass of the movable electrode, ε the dielectric constant of the gap medium, $A=b.L$ is the area of the microbeam and ω is the circular natural frequency. The gravitational acceleration is denoted g and F_0 is the non-dimensional magnitude of the shock. The natural period of the system is $T_p=0.02$ ms and is very small compared to the duration of the shock which is taken equal to 1 ms.

Fig. 18 is a reproduction of Fig. 17 for the considered microbeam but shown in the plane (V_{dc}, F_0). The grey zone corresponds to the set of parameters where the pull-in is suppressed.

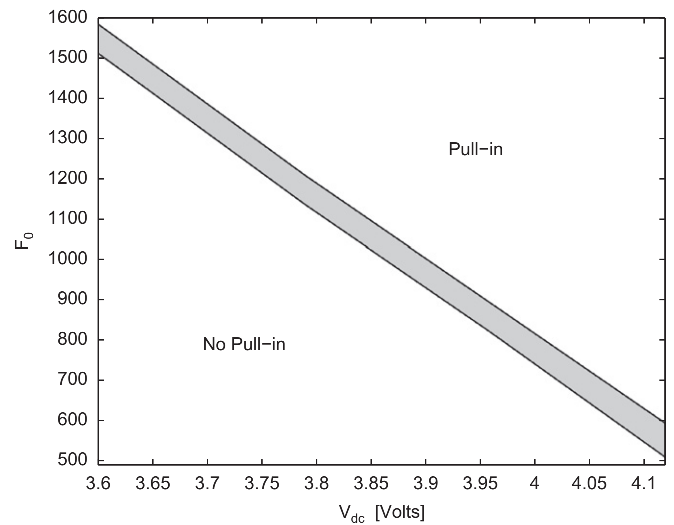

Fig. 18. Threshold of pull-in in the plane (V_{dc}, F_0) in the absence of HFV (lower curve) and in presence of HFV (higher curve). The grey zone is the zone where the pull-in is suppressed.

5. Conclusion

The effect of a high-frequency actuation on the occurrence of the pull-in instability, that can be caused by mechanical shocks and electrostatic forces, is studied analytically and numerically in this paper. A one dimensional lumped model was considered and the main equation governing the slow dynamic of the microstructure is derived by applying the method of direct partition of motion. The influence of a HFV on the pull-in phenomenon is investigated by analyzing the steady states solutions of the slow dynamic. It was shown analytically and numerically that when the microstructure is in the post pull-in state, induced by shocks and DC voltages, the introduction of a HFV creates stable solutions that can attract the movable electrode, and hence, avoid the failure of the device. The applicability of this result has been demonstrated in a real capacitive MEMS. The result of the present work indicates that a HFV offers an interesting possibility to suppress the pull-in instability keeping MEMS devices evolving in a safer environment. The HFV strategy used here for the quasi-static shock case can be extended to control the pull-in instability in the dynamic regime.

Acknowledgements

The authors would like to thank the anonymous reviewers for their constructive comments that improved the presentation of the paper.

References

[1] P. Osterberg, Electrostatically actuated microelectromechanical test structures for material property measurement, Ph.D. Thesis, MIT, 1995.
[2] M.I. Younis, E.M. Abdel-Rahman, A.H. Nayfeh, Static and dynamic behavior of an electrically excited resonant microbeam, in: Proceedings of the 43rd AIAA Structures, Structural Dynamics, and Materials Conference, Denver, CO, AIAA Paper, 2002, pp. 2002–1305.
[3] M. Abdel-Rahman, M.I. Younis, A.H. Nayfeh, A nonlinear reduced-order model for electrostatic MEMS, in: Proceedings of the 19th Biennial Conference in Mechanical Vibration and Noise (VIB), Chicago, IL, Paper DETC2003/VIB-48517, 2003 .
[4] J.A. Walraven, Future challenges for MEMS failure analysis, in: Proceedings of ITC International Test Conference, paper 33.4, 2003, pp. 850–855.
[5] M. Abdel-Rahman, M.I. Younis, A.H. Nayfeh, Characterization of the mechanical behavior of an electrically actuated microbeam, J. Micromech. Microeng. 12 (2002) 766–795.
[6] H.A. Tilmans, R. Legtenberg, Electrostatically driven vacuum-encapsulated polysilicon resonators. Part II. Theory and performance, Sens. Actuators A 45 (1994) 67–84.
[7] S. Krylov, R. Maimon, Pull-in dynamics of an elastic beam actuated by distributed electrostatic force, in: Proceedings of ASME Design Engineering Technical Conference Chicago, USA, paper DETC2003/Vib-48518, 2–6 September 2003.
[8] A.H. Nayfeh, M.I. Younis, Dynamics of MEMS resonators under superharmonic and subharmonic excitations, J. Micromech. Microeng. 15 (2005) 1840–1847.
[9] A.H. Nayfeh, M.I. Younis, E.M. Abdel-Rahman, Dynamic pull-in phenomenon in MEMS Resonators, Nonlinear Dyn. 48 (2007) 153–163.
[10] M.I. Younis, R. Miles, D. Jordy, Investigation of the response of microstructures under the combined effect of mechanical shock and electrostatic forces, J. Micromech. Microeng. 16 (2006) 2463–2474.
[11] M.I. Younis, F. Alsaleem, D. Jordy, The response of clamped–clamped microbeams under mechanical shock, Int. J. Non-linear Mech. 42 (2007) 643–657.
[12] M. Ibrahim, M.I. Younis, The dynamic response of electrostatically driven resonators under mechanical shock, J. Micromech. Microeng. 20 (2010) 025006.
[13] L. Castaner, J. Pons, R. Nadal-Guardia, A. Rodríguez, Analysis of extended actuation range of electrostatic actuators by current pulse drive, Sens. Actuators A, Phys. 90 (3) (2001) 181–190.

Author's personal copy

[14] J. Seeger, B. Boser, Charge control of parallel-plate, electrostatic actuators and the tip-in instability, J. Microelectromech. Syst. 12 (5) (2003) 656–671.
[15] S. Lenci, G. Rega, Control of pull-in dynamics in a nonlinear thermoelastic electrically actuated, microbeam, J. Micromech. Microeng. 16 (2006) 390–401.
[16] F. Lakrad, M. Belhaq, Suppression of pull-in instability in MEMS using a high-frequency actuation, Commun. Nonlinear Sci. Numer. Simulat. 15 (11) (2010) 3640–3646.
[17] J.J. Thomsen, Vibrations and Stability: Advanced Theory, Analysis, and Tools, Springer- Verlag, Berlin-Heidelberg, 2003.
[18] J.J. Thomsen, Some general effects of strong high-frequency excitation: stiffening, biasing, and smoothening, J. Sound Vib. 253 (2002) 807–831.
[19] J. Thomsen, Slow high-frequency effects in mechanics: problems, solutions, potentials, Int. J. Bifurcation and Chaos 15 (9) (2005) 2799–2818.
[20] B.P. Mann, M.A. Koplow, Symmetry breaking bifurcations of a parametrically excited Pendulum, Nonlinear Dyn. 46 (2006) 427–437.
[21] M. Bourkha, M. Belhaq, Effect of fast harmonic excitation on a self-excited motion in van der Pol oscillator, Chaos, Solitons & Fractals 34 (2) (2007) 621–627.
[22] M. Belhaq, A. Fahsi, 2: 1 and 1:1 frequency-locking in fast excited van der Pol-Mathieu-Duffing oscillator, Nonlinear Dyn. 53 (1–2) (2008) 139–152.
[23] M. Belhaq, A. Fahsi, Hysteresis suppression for primary and subharmonic 3: 1 resonances using fast excitation, Nonlinear Dyn. 57 (1–2) (2009) 275–287.
[24] J.F. Rhoads, S.W. Shaw, K.L. Turner, R. Baskaran, Tunable microelectromechanical filters that exploit parametric resonance, J. Vib. Acoust. 127 (5) (2005) 423–430.